NeuroImage

A novel method for functional brain networks based on static cerebral blood flow

--Manuscript Draft--

Manuscript Number:	
Article Type:	Full Length Article
Section/Category:	Analysis Methods
Corresponding Author:	Jinhui Wang, Ph.D. South China Normal University Guangzhou, Guangdong CHINA
First Author:	Changwen Wu
Order of Authors:	Changwen Wu
	Yu He
	Junle Li
	Xiaofan Qiu
	Qihong Zou
	Jinhui Wang, Ph.D.
Abstract:	Cerebral blood flow (CBF) offers a quantitative and reliable measurement for brain activity and is increasingly used to constructing functional networks. However, current methods evaluate inter-regional relations mainly based on CBF temporal dynamics, which suffers from low signal-to-noise ratio and poor temporal resolution. Here we proposed a method to construct CBF networks by estimating interregional Jensen-Shannon divergence-based similarity in regional distributions of static CBF measured by arterial spin labeling perfusion imaging over a scanning period. Based on CBF data of 30 healthy participants from 10 visits, we found that the CBF networks exhibited several non-trivial topological features (e.g., small-world organization, modular architecture, and hubs) and showed low-to-fair test-retest reliability and high between-subject consistency. We further found that interregional CBF similarities were depended on anatomical distance and differed between high- and lower-order subnetworks and nodal total CBF similarities were related to regional sizes and CBF levels. Finally, nodal CBF similarities were found to spatially align with the DAT and mGluR5 intensities, gene expression enriched in several cholesterol-related pathways, and cognitive processes related to language and executive functions. Altogether, CBF networks derived from our proposed method provide a reliable and neurobiologically meaningful means to study functional network organization of the human brain.
Suggested Reviewers:	Feng Liu Tianjin Medical University General Hospital fengliu@tijmu.edu.cn Expert in brain network methodology
	Xin Di New Jersey Institute of Technology synge.x.d@gmail.com Expert in brain network methodology
	Satoru Hayasaka hayasaka@utexas.edu Expert in brain network methodology
	Andrew Zalesky University of Melbourne azalesky@unimelb.edu.au Expert in brain network methodology
Opposed Reviewers:	

Highlight

Constructed CBF networks using divergence-based similarity in static CBF.

CBF networks showed non-trivial topology and high consistency across subjects.

CBF networks were influenced by anatomical distance, regional sizes, and CBF levels.

CBF networks correlated with genetic, chemoarchitectonic, and cognitive variables.

Abstract

Cerebral blood flow (CBF) offers a quantitative and reliable measurement for brain activity and is increasingly used to constructing functional networks. However, current methods evaluate inter-regional relations mainly based on CBF temporal dynamics, which suffers from low signal-to-noise ratio and poor temporal resolution. Here we proposed a method to construct CBF networks by estimating interregional Jensen-Shannon divergence-based similarity in regional distributions of static CBF measured by arterial spin labeling perfusion imaging over a scanning period. Based on CBF data of 30 healthy participants from 10 visits, we found that the CBF networks exhibited several non-trivial topological features (e.g., small-world organization, modular architecture, and hubs) and showed low-to-fair test-retest reliability and high between-subject consistency. We further found that interregional CBF similarities were depended on anatomical distance and differed between high- and lower-order subnetworks and nodal total CBF similarities were related to regional sizes and CBF levels. Finally, nodal CBF similarities were found to spatially align with the DAT and mGluR5 intensities, gene expression enriched in several cholesterol-related pathways, and cognitive processes related to language and executive functions. Altogether, CBF networks derived from our proposed method provide a reliable and neurobiologically meaningful means to study functional network organization of the human brain.

Keywords: brain network, cerebral blood flow, arterial spin labeling, gene

expression, neurotransmitter

Introduction

Functional connectivity has become an effective method for characterizing intrinsic functional dynamics (Van Dijk et al., 2010) and been applied to assess variations in neuropsychiatric disorders (Li et al., 2022; Liu et al., 2017; Wang et al., 2013), cognitive ability (Li et al., 2017; Sripada et al., 2021), and development (Gao et al., 2017). Currently, functional connectivity is estimated mainly based on blood oxygen level-dependent (BOLD) signals measured by functional magnetic resonance imaging (fMRI). However, BOLD signals are an indirect index for neuronal activity, which measure hemodynamic changes influenced by cerebral blood flow (CBF), blood volume, and blood oxygenation (Hillman, 2014). By contrast, CBF as measured by arterial spin labeling (ASL) perfusion imaging is a direct and quantitative biological index for brain function (Wang et al., 2008; Wong, 2014). Moreover, CBF couples with cerebral metabolic rates for glucose and oxygen consumption (Vaishnavi et al., 2010a). Therefore, CBF may serve as an ideal data source to assess functional connectivity.

To date, several methods have been proposed to estimate functional connectivity based on CBF. For example, an early study applied independent component analysis to CBF time series and identified 5 distinct resting-state networks with spatial and temporal characteristics closely matched those derived from BOLD-based functional networks (De Luca et al., 2006). Subsequently, Liang et al. constructed functional networks by calculating Pearson correlation of regional CBF time series and found that the hub regions largely overlapped with those in BOLD-based functional

networks (Liang et al., 2014). The Pearson correlation-based method can also be extended to multiple regression (Li et al., 2020) and cross-correlation (Zou et al., 2009). Despite the success, it should be noted that such CBF time series-based functional connectivity methods are limited by the low signal-to-noise ratio and poor temporal resolution of CBF time series (Alsop et al., 2015; Wong, 2014; Zou et al., 2009). This largely limits the application scenarios of these CBF time series-based functional connectivity methods. Accordingly, it is necessary to develop more appropriate methods for studying functional connectivity or networks using CBF.

Here, we proposed a novel method to construct CBF networks based on the static mean perfusion map over a scanning period. Previous studies have shown that the static mean perfusion map has high signal-to-noise ratio and exhibits high test-retest (TRT) reliability (Zou et al., 2015). Specifically, we employed a kernel density estimation method to fit regional CBF distributions, between which the similarity was quantified by Jensen-Shannon divergence-based approach. For the resulting CBF networks, we systematically characterized their topological architecture, evaluated their TRT reliability, between-subject consistency, and potential influencing factors, and explored their chemoarchitectonic, genetic, and cognitive correlates. Our results indicate that the proposed method for CBF networks offers a relatively reliable, neurobiologically meaningful, and cognitively relevant means for future functional connectome studies.

Materials and Methods

Participants and data acquisition

A publicly available TRT dataset was used in this study (Chen et al., 2015). This dataset contained 30 subjects (15 females; mean age 24, SD = 2.41), who were confirmed to have no history of neurological or psychiatric disorders, substance abuse, or head injuries resulting in consciousness loss. Each subject was scanned ten times over one month with one scan every three days. Specifically, ASL perfusion MRI data were acquired using a 3.0-Tesla Discovery MR750 scanner (General Electric, Milwaukee, WI, USA), employing a 3D pseudo-continuous arterial spin labeling sequence with the following parameters: TR = 4.834 s; TE = 11.088 ms; FA = 111°; slice thickness = 3 mm; no gap; slice number = 100; matrix = 128 × 128; FOV = 100% of phase FOV. A T1-weighted Fast Spoiled Gradient echo (TR = 8.1 ms, TE = 3.1 ms, TI = 450 ms, flip angle = 8°, field of view = 256 × 256 mm^2, matrix = 256 × 256, voxel size = 1.0 × 1.0 × 1.0 mm^3, and 176 sagittal slices) was carried out to acquire a high-resolution anatomical image of the brain structure. A written informed consent was obtained from each subject before data collection. For more details, see (Chen et al., 2015).

Preprocessing of ASL images

For the ASL perfusion MRI, individual CBF-weighted images were obtained using Function Tool (AW 4.5 Workstation; GE Healthcare). The CBF-weighted images were then corrected for partial volume effects using the ASLtbx toolbox (Hu et al., 2010; Wang et al., 2008), co-registered to corresponding structural images,

normalized to the MNI space, resampled to 3-mm isotropic voxels, and spatially smoothed using a 6-mm full-width half-maximum Gaussian kernel. Finally, the CBF-weighted images were mean-scaled by dividing each voxel's value by the whole-brain mean value for each subject.

Construction of CBF networks

Definition of network nodes. The network nodes were defined by Schaefer's atlas, which parcels the cerebral cortex into 200 regions of interest (ROIs) (Schaefer et al., 2018). Specifically, these ROIs were categorized into seven subnetworks (Thomas Yeo et al., 2011): visual network (VN), somatomotor network (SMN), dorsal attention network (DAN), ventral attention network (VAN), limbic network (LN), fronto-parietal control network (FPN), and default mode network (DMN).

Definition of network edges. The network edges were defined as Jensen-Shannon divergence-based similarity (JSDs) to quantify the similarity of CBF distributions of two brain regions. We first extracted CBF signals within each region and estimated the probability density function (using MATLAB function *ksdensity*). The probability density functions were then transformed into probability distributions (PDs). Finally, the JSDs was defined by:

$$JSDs(P,Q) = 1 - \sqrt{JSD(P||Q)}.$$

$$JSD(P||Q) = \frac{1}{2}\sum_{i=1}^{n} P(i) log \frac{P(i)}{M(i)} + \frac{1}{2}\sum_{i=1}^{n} Q(i) log \frac{Q(i)}{M(i)}.$$

$$M = \frac{1}{2}(P+Q).$$

where P and Q denote regional PDs, and n denotes the sample points number (2^8 in

this study) (Wang et al., 2016). The value range for JSDs is [0, 1], a higher value indicates higher similarity.

Graph-based topological characterization of CBF networks

We utilized graph-based network measures to characterize CBF networks. All network analyses were performed with the GRETNA toolbox (Wang et al., 2015).

Threshold selection. A sparsity-based thresholding procedure was used to binarize networks, ensuring the same edge number across subjects and scans. The sparsity was defined as the ratio of the actual edge number to the maximum possible edge number in the network (20 logarithmically spaced values from 0.05 to 0.95 in this study).

Global properties. We calculated five global properties (clustering coefficient, C_p, shortest path length, L_p, local efficiency, E_{loc}, global efficiency, E_{glob}, and modularity, Q) at each sparsity for each network. Considering the dependence of network properties on sparsity, we further calculated the area under the curve (AUC) to provide summary scalars. To test whether the CBF networks are non-randomly organized, all global properties were further normalized by dividing them by the corresponding average of the 100 matched random networks. These random networks were generated using a topological rewiring algorithm to preserve the same degree distribution as the original networks (Maslov and Sneppen, 2002). Typically, a small-world, highly efficient, and modular network should fulfill the following conditions: normalized $C_p > 1$ and normalized $L_p \sim 1$, normalized $E_{loc} > 1$ and normalized $E_{glob} \sim 1$, and normalized $Q > 1$.

Nodal properties. We calculated the nodal degrees at each sparsity and used AUC as the summary scalar for each network. In addition, we averaged the nodal degrees across all networks, to fit the degree distribution using different models (power law, exponential, and exponentially truncated power law) and identified hubs as regions whose nodal degree ranked in the top 10%.

Evaluation of CBF networks

TRT reliability. We quantified the TRT reliability of the CBF networks using intraclass correlation coefficient (ICC) (Shrout and Fleiss, 1979). Specifically, we focused on the global properties, nodal degrees, and edges of the CBF networks. For a given measure repeatedly observed *k* times, the ICC was calculated as:

$$ICC = \frac{MS_R - MS_W}{MS_R + (k-1)MS_W} ,$$

where MS_R represents the mean square of between-subject variance; MS_W represents the mean square of within-subject variance; and *k* represents the number of repeated observations per subject (here, *k* =10). Similar to our previous studies (Wang et al., 2011, 2016; Y. Li et al., 2021; Yin et al., 2023), the TRT reliability was categorized as poor (ICC < 0.25), low (0.25 < ICC < 0.4), fair (0.4 < ICC < 0.6), good (0.6 < ICC < 0.75), and excellent (0.75 < ICC < 1).

Between-subject consistency. The networks and the nodal degrees were averaged across ten scans and then assessed by Pearson correlation for each pair of subjects, measuring their between-subject consistency.

Inter-subnetwork differences. To study whether the CBF networks were related to

functional topography of the cortex, we categorized the seven subnetworks predefined in the Schaefer's atlas into low-order (VN and SMN) and high-order (DAN, VAN, FPN, and DMN) subnetworks (Stanford et al., 2022). After averaging the CBF networks across subjects, we evaluate the differences between low- and high-order subnetworks in nodal degree, within-subnetwork interregional CBF similarity using a nonparametric permutation test based on two-sample *t*-tests (10,000 times).

Potential influencing factors. After averaging the CBF networks and their nodal degrees across all subjects and scans, we used Spearman correlation to assess the relationships (1) between the regional sizes and the nodal degrees; (2) between the average regional CBF levels and the nodal degrees; and (3) between the interregional anatomical distances (Euclidean distance) and CBF similarities; The significance levels of these correlations were estimated with nonparametric spin-based permutation tests (10,000 repetitions) (Alexander-Bloch et al., 2018; Váša et al., 2018). The spin-based permutation test is a widely used approach to measure the significance of the correlation between two cortical maps (the source and target maps) while correcting for spatial autocorrelation. Specifically, random rotation is first applied to the spherical projection of parcellation. Then, the source map is permuted according to the order of the rotated brain regions. Next, the correlation coefficient is calculated between the target map and the permuted source map, generating a null distribution after 10,000 repetitions. Finally, the *P*-value is obtained as the proportion of permutations where the resultant absolute values of coefficients equaled or exceeded the actual absolute value of the coefficient between the target map and the

source map.

Chemoarchitectonic correlates of CBF networks

To investigate the chemoarchitectonic correlates of the CBF networks, we obtained data from https://github.com/netneurolab/hansen_receptors/tree/main/data/PET_parcellated (Hansen et al., 2022), which provided 38 neurotransmitter intensity maps of healthy subjects from multiple studies, including: 5-HT_{1A}, 5-HT_{1B}, 5-HT_{2A}, 5-HT_4, 5-HT_6, 5-HTT, $\alpha_4\beta_2$, CB_1, D_1, D_2, DAT, $GABA_A$, H_3, M_1, $mGluR_5$, MOR, NET, NMDA, and VAChT. The D2 intensity map using raclopride tracers was excluded from further analysis due to the unreliable binding of raclopride tracers in the cortex. Details on these neurotransmitter intensity maps can be found at https://github.com/netneurolab/neuromaps/wiki/Annotation-information (Markello et al., 2022). We then analyzed the relationship between the nodal degrees of the CBF networks and the regional mean intensities of each neurotransmitter using Spearman correlation, after averaging the nodal degrees across all subjects and scans. All correlations were validated using nonparametric spin-based permutation tests (10,000 times). A false discovery rate (FDR) procedure was employed to correct for multiple comparisons across all correlations at the level of $q < 0.05$.

Genetic correlates of CBF networks

To investigate the genetic correlates of the CBF networks, we examined the

correlation between the nodal degrees of the CBF networks and transcriptional profiles from the AHBA dataset. For genes that strongly contributed to the correlation, we further performed gene ontology (GO) enrichment analysis to identify their relevant biological process.

AHBA dataset. The AHBA dataset is a publicly available online resource, which contains brain-wide transcriptomic information and multimodal MRI obtained from six healthy adult human donors (age, 24 - 57 years; 5 males and 1 female) with no known neuropathological or neuropsychiatric disease history (Hawrylycz et al., 2012). Specifically, the transcriptional activity was recorded for 20,737 genes from 3,702 spatially distinct tissue samples that covered almost the entire brain. The tissue samples were collected from the left hemisphere for 4 donors and both hemispheres for 2 donors. For more details, see http://human.brain-map.org/.

Gene data preprocessing. Standardized workflows (Arnatkevičiūtė et al., 2019) were used to preprocess the gene data in the AHBA dataset with the abagen toolbox (version 0.1.3; https://github.com/rmarkello/abagen) (Markello et al., 2021). First, we applied intensity-based filtering to exclude probes that did not exceed background noise in more than 50% of the samples. Then, a representative probe was selected for each gene with the most consistent pattern of regional variations across the six donor brains as quantified by Differential Stability (Hawrylycz et al., 2016; Kirsch and Chechik, 2016). To assign gene expression samples to the regions, we excluded samples further than 2 mm away from any voxel in the parcellation and assigned each of the remaining samples to its nearest region according to the minimum distance

between the sample and any voxel in a region. Finally, gene expression levels of the remaining samples were normalized for each donor by applying a scaled robust sigmoid normalization for every sample across genes and for every gene across samples to assess the relative expression of each gene across regions while controlling for donor-specific differences in gene expression. To obtain regional gene expression profiles, the normalized expressions for samples assigned to the same region were averaged for each donor and aggregated into a region × gene matrix comprising expression levels of 15,633 genes over 200 regions.

Relationship between CBF networks and transcriptional profiles. To investigate the relationship between CBF networks and transcriptional profiles, we performed the partial least squares (PLS) regression to predict the group-level mean nodal degrees of the CBF networks with regional expression levels of all genes. The PLS1 was the linear combination of regional expression levels of all genes that exhibited the strongest correlation with the nodal degrees. The significance level of the correlation was estimated by re-running the PLS regression for nodal degrees simulated via a nonparametric spin-based permutation test (10,000 times) to correct for spatial autocorrelation. If a significant correlation was observed, the weights of all genes to form the PLS1 were *Z*-transformed, and genes with an absolute *Z*-score > 1.64 were considered to contribute to the correlation strongly. Furthermore, to investigate whether the nodal degrees of the CBF networks are related to the cellular architecture-specific gene expressions, we performed Spearman correlations between the nodal degrees and mean gene expressions of canonical cell classes, including excitatory

neurons, inhibitory neurons, oligodendrocyte progenitor cells, astrocytes, endothelial cells, microglia, and oligodendrocytes (Arnatkeviciute et al., 2021). All correlations were subsequently validated using nonparametric spin-based permutation tests (10,000 times). Finally, the FDR procedure was applied to correct for multiple comparisons across seven cell classes at the level of $q < 0.05$.

GO enrichment analysis. For the identified genes that strongly contributed to the PLS1, we performed GO enrichment analysis to search for their related GO terms, this analysis were performed separately for the genes showing the strongest positive and negative contributions to the component (i.e., PLS1+ and PLS1- genes). First, we downloaded the biological process-related GO term hierarchy and annotation files for Homo sapiens (version April 17, 2019) from https://figshare.com/s/71fe1d9b2386ec05f421 (Fulcher et al., 2021). Then, we ran the gene-to-category annotations, processed the hierarchy correlations between GO terms, and restricted our analysis to the GO terms with 10 - 1,000 gene annotations (Vértes et al., 2016; Whitaker et al., 2016). A spatial ensemble null model was used to reduce the false-positive rate in GO enrichment analysis (Fulcher et al., 2021). Specifically, an enrichment coefficient was calculated for each resulting GO term. To estimate the significance levels of the enrichment coefficients, we re-ran the PLS regression for the nodal degrees simulated via nonparametric spin-based permutation (Alexander-Bloch et al., 2018; Váša et al., 2018) and re-calculated the enrichment coefficient for each GO term. Significant GO terms were determined after correcting for multiple comparisons with the Bonferroni procedure at the level of $p < 0.05$, followed by

removing redundant GO terms with the online tool REViGO (http://revigo.irb.hr, version 1.8.1, May 10, 2023) (Supek et al., 2011). Notably, the GO enrichment analysis was performed for genes that contribute to the correlations positively and negatively, respectively.

Cognitive correlates of CBF networks

To examine the cognitive correlates of CBF networks, we correlated the averaged degree of CBF networks across all subjects and scans with multiple cognitive association test maps using PLS regression. The cognitive association test maps were derived from the NeuroSynth database (Yarkoni et al., 2011) (https://github.com/neurosynth/neurosynth), and quantitatively represented how regional fluctuations in activity were related to specific cognitive processes. Specifically, a total of 123 cognitive association test maps that primarily focused on cognitive function were selected based on the Cognitive Atlas (Poldrack et al., 2011). The full list of these maps can be found in (Hansen et al., 2022). The selected maps were further parcellated using the Schaefer atlas and Z-transformed to generate the cognitive association test scores at the regional level for the PLS regression. To estimate the significance level of the PLS regression, a nonparametric spin-based permutation test was used (10,000 times) (Alexander-Bloch et al., 2018; Váša et al., 2018). If a significant correlation was observed, we computed the Pearson correlation coefficient between each association test map and the PLS1, the linear combination of cognitive association test maps that exhibited the strongest correlation with the nodal

degrees. All correlations were validated using nonparametric spin-based permutation tests (10,000 times). The association test maps with significantly positive/negative correlation coefficients were considered to positively/negatively contribute to the PLS1, after the Bonferroni correction procedure across all correlations at the level of $p < 0.05$.

Results

Connectivity and topological organization of CBF networks

Connectivity patterns. Figure 1a shows the group-level mean CBF network. The group-level mean CBF network exhibited high interregional CBF similarities with low variance (0.708 ± 0.096).

Global properties. Each subject's CBF network exhibited typical small-worldness, high efficiency, and modular architecture over the whole thresholding range, as evidenced by normalized $C_p > 1$ and normalized $L_p \sim 1$, normalized $E_{loc} > 1$ and normalized $E_{glob} \sim 1$, and normalized $Q > 1$ (Figure 1b).

Nodal properties. The exponentially truncated power law model gave the best fitting to the degree distribution of the CBF networks ($R^2 = 0.985$) (Figure 1c). A total of 20 hubs were identified that were predominantly located in the DAN (5), DMN (5), SMN (4), and VAN (4) (Figure 1d**)**.

Assessment of reliability and influences on structure of CBF networks

Reliability and consistency. Global network attributes of the CBF networks exhibited low TRT reliability (C_p: ICC = 0.347; L_p: ICC = 0.200; E_{loc}: ICC = 0.345;

E_{glob}: ICC = 0.277; Q: ICC = 0.259). For nodal degree, although most regions exhibited low TRT reliability (ICC = 0.206 ± 0.102), a specific set of regions (9, 4.5%) showed fair TRT reliability (Figure 2a), which were predominantly located in the VAN (4, 44.4%) and DMN (3, 33.3%) such as the right temporal-occipital-parietal junction region and left prefrontal cortex. Similarly, despite an overall low TRT reliability for interregional CBF similarity, a specific subset of edges (888, 4.46%) showed fair TRT reliability (Figure 2b). Both nodal degrees (r = 0.746 ± 0.103) (Figure 2c) and interregional CBF similarities (r = 0.654 ± 0.112) (Figure 2d) showed high consistency among subjects.

Inter-subnetwork differences. The high-order subnetworks exhibited significantly higher intra-network CBF similarities compared to the low-order subnetworks (t = 7.740, $p < 0.001$) (Figure 3). No significant differences were observed for nodal degrees between the high- and low-order subnetworks (t = 0.860, p = 0.383).

Potential influencing factors. We found that the interregional CBF similarities were significantly correlated with anatomical distance (rho = -0.239, $p < 0.001$) (Figure 4a), Moreover, the nodal degree of the CBF networks was significantly correlated with regional size (rho = -0.339, $p < 0.001$, Figure 4b), and regional mean CBF level (rho = 0.601, $p < 0.001$, Figure 4c).

Association between neurotransmitter intensities and nodal degrees of CBF networks

Significantly correlations were observed between the nodal degrees of CBF networks

and the intensity of DAT with [^{11}C]P943 tracer (*rho* = 0.266, $p < 0.001$) (Figure 5a) and mGluR5 with [^{11}C]ABP688 tracer (*rho* = -0.367, $p = 0.002$) (Figure 5b).

Mapping nodal degrees of CBF networks to gene expression

A significantly positive correlation was observed between the nodal degrees of the CBF networks and regional gene expression profiles, the PLS1 explained 28% of the variance of the nodal degrees ($r = 0.530$, $p = 0.043$) (Figure 6a). A total of 810 genes were considered as strong contributors to this correlation (PLS1+: 427 genes; PLS1-: 383 genes, Figure 6b). After redundant GO terms were removed with REVIGO, GO enrichment analysis revealed that the PLS1+ genes were enriched in 17 biological processes which encompassed a diverse range of cellular activities, primarily involved in the cholesterol-related process (e.g., “intracellular cholesterol transport”, “cholesterol homeostasis), and PLS1- genes were not enriched in any neurobiological processes. Detailed information about these biological processes was provided in Table S1. After multiple comparison correction, the nodal degrees of the CBF networks showed a positive correlation with the mean expression of the genes enriched in endothelial cells (*rho* = 0.332, $p < 0.001$) (Figure 6c).

Mapping nodal degrees of CBF networks to cognitive function

We observed a significant correlation between the nodal degrees of the CBF networks and cognitive association test maps, with 32.8% of the variance of the nodal degrees explained by PLS1 ($r = 0.573$, $p = 0.003$). A total of 52 cognitive processes were

considered as strong contributors to this correlation (positive contributors: 24 cognitive processes; negative contributors: 28 cognitive processes). The cognitive processes with the six highest positive correlation coefficients were mainly enriched in executive functions (e.g., ‘goal’, ‘monitoring’, ‘interference’, ‘response selection’, and ‘planning’), and ‘working memory’ and the cognitive processes with the six highest negative correlation coefficients were primarily enriched in the language domain, such as ‘communication’, ‘meaning’, ‘listening’, ‘language comprehension’, ‘speech perception’, and ‘language’ (Figure 7).

Discussion

In this study, we introduced a JSDs method to construct CBF networks that eliminated the need to acquire CBF time series. We systematically investigated the CBF networks by analyzing their topological structure, reliability, and associations with chemoarchitecture, gene expression, and cognition. We first found that the CBF networks exhibited non-trivial organization. Further analysis revealed low-to-fair TRT reliability and high consistency among subjects of the CBF networks. We also demonstrated that the CBF networks were modulated by regional size and CBF level, anatomical distance, and functional cortical topography. Finally, we observed significant correlations of the CBF networks with DAT and mGluR5, gene expression enriched in cholesterol-related pathways, and language and executive processes. Altogether, this study offers a relatively reliable and biologically meaningful framework for constructing CBF networks, providing a new way for future research

on functional connectome of the human brain.

The nontrivial organization of CBF networks

Our findings revealed that the CBF networks exhibited small-world topology that was thought to support the efficient segregation and integration of information in the human brain while minimizing wiring and energy costs (Bassett and Bullmore, 2006; Liao et al., 2017). This principle is also observed in other brain networks, such as BOLD-based functional networks (Wang et al., 2009a), structural networks (Hagmann et al., 2007), and morphological networks (Y. Li et al., 2021; Wang et al., 2016), reinforcing the idea that the small-world topology is a common feature across different brain networks. We also found that the CBF network exhibited modular organization. Modular organization in the brain refers to the idea that neural networks are divided into several distinct, interacting subnetworks or modules. This organization allows the brain to efficiently process information by localizing certain functions to specific modules while maintaining inter-module communications, thus improving the robustness, adaptivity, and evolvability of network and, supporting the emergence of adaptive behavior and cognition (Bullmore and Sporns, 2009; Meunier et al., 2010). Considering the functionally defined and Yeo-7 subnetworks-based atlas, i.e., Schaefer's atlas, used for CBF network construction, an interesting question is raised that how the functional modules interacts in CBF networks, which will deepen our understanding on how the CBF networks support human brain functions. Moreover, we identified several interconnected hubs of the CBF networks and found a

significant positive correlation between nodal degrees and the regional CBF levels, suggesting that hubs of the CBF networks received higher CBF. Regions with high CBF levels are typically associated with enhanced neuronal activity, dense capillary networks, and increased energy demands for oxygen and glucose (Karbowski, 2011; Watts et al., 2018). These features make them more likely to participate in neural processing, which may explain their role as hub nodes in the CBF networks.

Moderate reliability of CBF networks

In this study, we evaluated the TRT reliability and between-subject consistency of CBF networks. We observed that the ICC values of interregional CBF similarity and nodal degree ranged from low to fair. Previous studies have shown that the human CBF is affected by physical and emotional states of participants (Honda et al., 2018; Hoshi and Chen, 2002; Ozawa et al., 2019) and the morning-evening variation (Shannon et al., 2013). These factors are thus speculated to lead to, to some extent, the observed low-to-fair TRT reliability of CBF networks. In addition to these factors, different image preprocessing strategies are previously reported to influence the TRT reliability of CBF signals, such as motion correction and spatial filtering (Fazlollahi et al., 2015). Therefore, future studies are needed to examine how different image preprocessing strategies affect the TRT reliability of CBF networks, which will provide guidance on determining analytical strategies for obtaining reliable CBF networks. Meanwhile, the factors of brain parcellation, thresholding method, and network type, which are demonstrated to affect the TRT reliability of brain networks

(Garrison et al., 2015; Y. Li et al., 2021; Wang et al., 2009b, 2011; Yin et al., 2023), should also be taken into account in future. Despite the low-to-fair TRT reliability, we observed high consistency across subjects for the CBF networks in terms of both nodal degree and interregional CBF similarity. The high consistency suggests the presence of a stable, intrinsic CBF network patterning shared across subjects. Thus, we averaged individual CBF networks to derive a consensus estimate of the CBF network structure, which was used to explore their neurobiological signatures.

Neurobiological signatures of CBF networks

We examined neurobiological signatures of CBF networks by linking them with chemoarchitecture and transcriptional profiles. We observed a positive correlation between the degree of CBF networks and dopaminergic neurotransmitter intensity (DAT), while finding a negative correlation with glutamatergic activity (mGluR5). A previous study demonstrated that CBF changes induced by different psychiatric medications are associated with neurotransmitter systems, including DAT (Dukart et al., 2018). Regarding mGluR5, its activation triggers Ca^{2+} transients in astrocytes (Wang et al., 2006), which initiates a series of events that ultimately modulate CBF through the regulation of arteriole smooth muscle tone (Zonta et al., 2003). Thus, the observed associations of CBF networks with DAT and mGluR5 might be driven by the modulatory effects of these neurotransmitters on CBF dynamics.

In addition to the chemoarchitectonic analysis, we showed that the CBF networks significantly correlate with transcriptional profile and identified genes with strong

contributions to this correlation. Subsequent analyses revealed that these genes were primarily enriched in cholesterol-related processes, including intracellular cholesterol transport and cholesterol homeostasis which refer to the cholesterol movement within cells and the process involved in the maintenance of a steady state of cholesterol, respectively. These two terms collectively underscore the regulatory balance of cholesterol. Physiologically, cholesterol plays a critical role in maintaining the optimal level of energetic metabolism (Czuba et al., 2017). Considering that the CBF is deemed as closely coupled with glucose and oxygen metabolism (Hoge et al., 1999; Paulson et al., 2010; Vaishnavi et al., 2010b), and has been used as a surrogate of energetic metabolism (Liang et al., 2013), the observed relationship of CBF networks with cholesterol-related processes in this study may reflect a potential collaboration between cholesterol regulation and CBF distribution in supporting brain energy demands. In addition to the cholesterol-related processes, the PLS1+ genes were also enriched in several endothelial cell-related processes (e.g., positive regulation of endothelial cells apoptotic process and regulation of endothelial cells differentiation), which mirrored the finding of a significant correlation between nodal degrees and mean gene expressions of genes enriched in endothelial cells. For endothelial cells, several studies have reported its role in CBF regulation, including vascular tone regulation, inflammatory response, thrombosis, adhesion, and vascular permeability (Ashby and Mack, 2021; Cohen, 1995; Godo and Shimokawa, 2017). Hence, this finding suggests that the CBF networks may capture the affiliation between endothelial cells and the CBF circulation. Taken together, our findings provide new

insights into understanding the neurobiological substrates of CBF networks by linking the macroscopic topology of the CBF networks with various microscopic biological processes.

Cognitive and behavioral relevance of CBF networks

In this study, we demonstrated the cognitive and behavioral relevance of CBF networks using a multivariate mapping method. Numerous studies have pointed out that the cognition results from the functional interactions of distributed brain systems operating in large-scale networks (Bressler and Menon, 2010). Noticing the non-random modular organization exhibited in the CBF networks, it is interesting in the future to characterize the modular architecture of CBF networks in detail, and further investigate the roles of interactions between and within these modules on human cognition. Such study can significantly advance our understanding on how CBF networks support cognition. Specifically, the cognitive functions largely contributing to the mapping between CBF networks and cognitive and behavioral data included executive function, working memory, and language processing. This finding is aligned with a cohort study that higher regional CBF levels are associated with better performance in attention, executive function, and memory (Leeuwis et al., 2018), suggesting that cognitive performance is not only linked to regional CBF levels but also to topological organization of the CBF networks. Altogether, our findings provide a network-based perspective on how CBF modulates cognitive processes, and bring a new insight into the neural mechanisms underlying cognition.

Limitations and future directions

Several limitations existed in the current study. First, there were inherent issues associated with ASL imaging technology, e.g., the inevitably intravascular artifacts. Although inflow saturation was implemented to suppress the intravascular signal results from the inflow of blood during post-labeling delay, we could not fully exclude the influence of this issue on the CBF networks. Further technical progress is needed to resolve these issues for constructing more reliable CBF networks. Second, the biological meaning of CBF networks was examined by associating the networks with publicly available datasets. This may result in an underestimation of the genetic and chemoarchitectonic correlates of CBF networks. Therefore, further work is required by collecting the related data from the same cohort of participants to validate our results. Finally, CBF alterations have been found in several neuropsychiatric disorders (Falcon et al., 2024; R. Li et al., 2021; Percie Du Sert et al., 2023), an interesting topic in the future is to investigate whether CBF networks are also disrupted in these disorders.

Data availability statement

The data that support the findings of this study are available from the corresponding author upon reasonable request.

Acknowledgements

This work was supported by the National Natural Science Foundation of China (No. 82472092), grant from Research Center for Brain Cognition and Human Development, Guangdong, China (No. 2024B0303390003), STI 2030—Major Projects (No. 2021ZD0200500), National Social Science Foundation of China (No. 20&ZD296), Key-Area Research and Development Program of Guangdong Province (2019B030335001), and Striving for the First-Class, Improving Weak Links and Highlighting Features (SIH) Key Discipline for Psychology in South China Normal University.

Competing interests

The authors declare no competing interests.

Figure legends

Figure 1. Topological organization of the CBF networks. **a)** Group-level mean CBF similarity matrix. **b)** The CBF networks showed small-world organization, high parallel efficiency, and modularity. **c)** The degree distribution of the CBF networks was best fitted by the exponentially truncated power law model. **d)** A total of 20 regions were identified as hubs in the CBF networks. CBF, cerebral blood flow; JSDs, Jensen-Shannon divergence-based similarity; Nor $C_{p,}$ normalized clustering coefficient; Nor L_p, normalized shortest path length; Nor E_{loc}, normalized local efficiency; Nor E_{glob}, normalized global efficiency; Nor $Q,$ normalized modularity; LH, left hemisphere; RH, right hemisphere; FrOper, frontal operculum; Ins, insula; PFCl, lateral prefrontal cortex; pCunPCC, precuneus posterior cingulate cortex; Temp, temporal.

Figure 2. The test-retest reliability and between-subject consistency of the CBF networks. The CBF networks exhibited low-to-fair test-retest reliabilities and high between-subject consistencies for both nodal degree (**a** and **c**) and interregional CBF similarity (**b** and **d)**. TRT, test-retest; CBF, cerebral blood flow; ICC, intraclass correlation coefficient.

Figure 3. The difference between high- and low-order subnetworks in interregional CBF similarity. Significantly higher interregional CBF similarity was found within high- than low-order subnetworks**.** CBF, cerebral blood flow.

Figure 4. Factors affecting the CBF networks. **a)** Interregional CBF similarities exhibited a significantly negative correlation the anatomical distances between regions. **b)** Nodal degrees of the CBF networks showed a significantly negative correlation with regional sizes. **c)** Nodal degrees of the CBF networks showed a significantly positive correlation with regional CBF levels. CBF, cerebral blood flow.

Figure 5. Chemoarchitectonic correlates of the CBF networks. Nodal degrees of the CBF networks showed a significantly positive correlation with regional intensities of DAT (**a**) and a significantly negative correlation with regional intensities of mGluR5 (**b**).

Figure 6. Genetic correlates of the CBF networks. **a)** Nodal degrees of the CBF networks showed a significantly positive correlation with the PLS1 scores derived from transcriptional activity of 15,633 genes. **b)** A total of 427 and 383 genes were identified to show positive and negative contribution to the PLS1 scores, respectively. **c)** Nodal degrees of the CBF networks showed a significantly positive correlation with the mean transcriptional activity of genes enriched in the endothelial cell. PLS, partial least-squares; FDR, false discovery rate.

Figure 7. Cognitive relevance of the CBF networks**. a)** Nodal degrees of the CBF networks showed a significantly positive correlation with the PLS1 scores derived

from 123 activation maps. **b)** A total of 24 and 28 cognitive processes were identified to show positive and negative contribution to the PLS1 scores, respectively. PLS, partial least-squares.

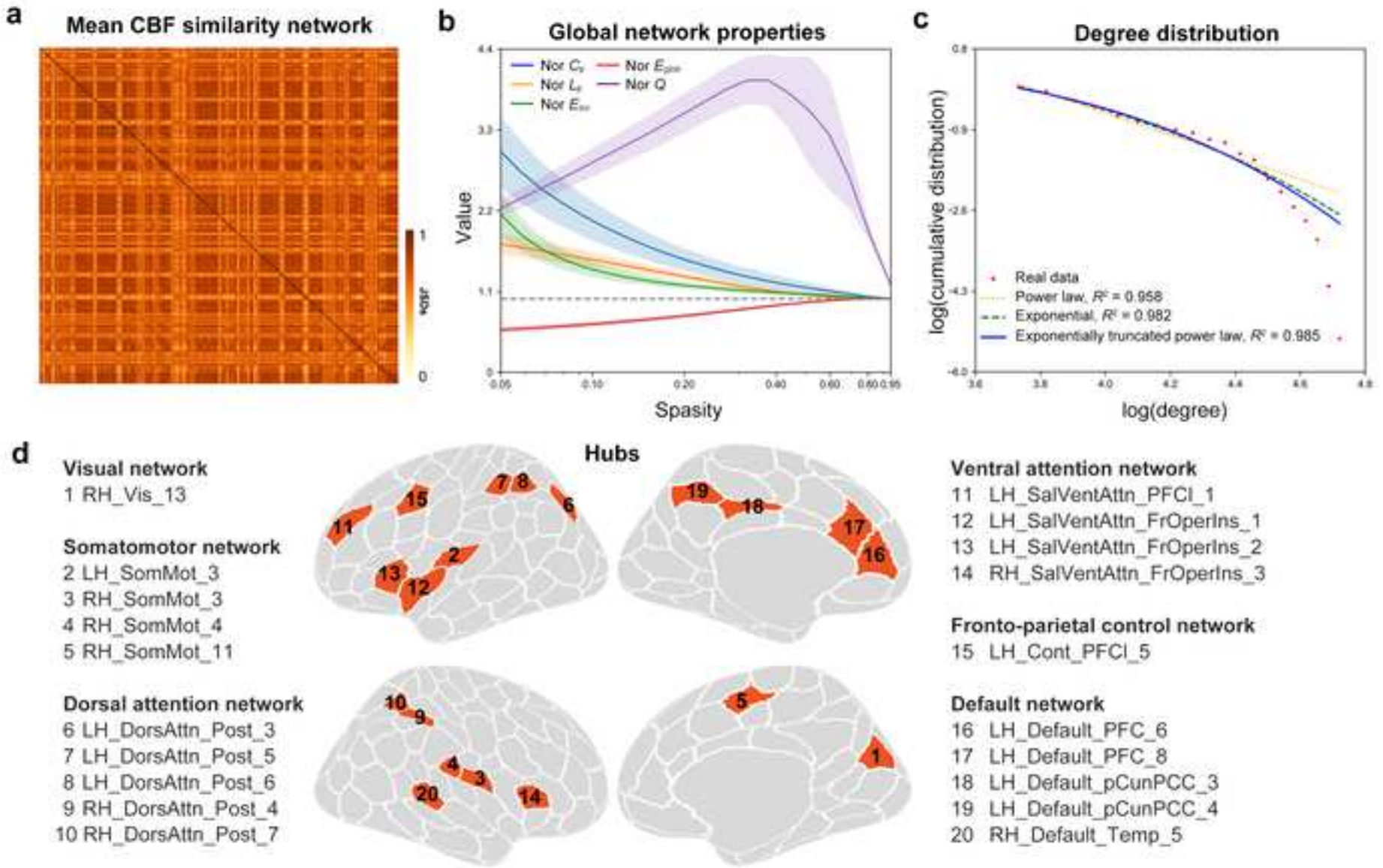

9. Figure

Click here to access/download;9. Figure;Figure2.tif

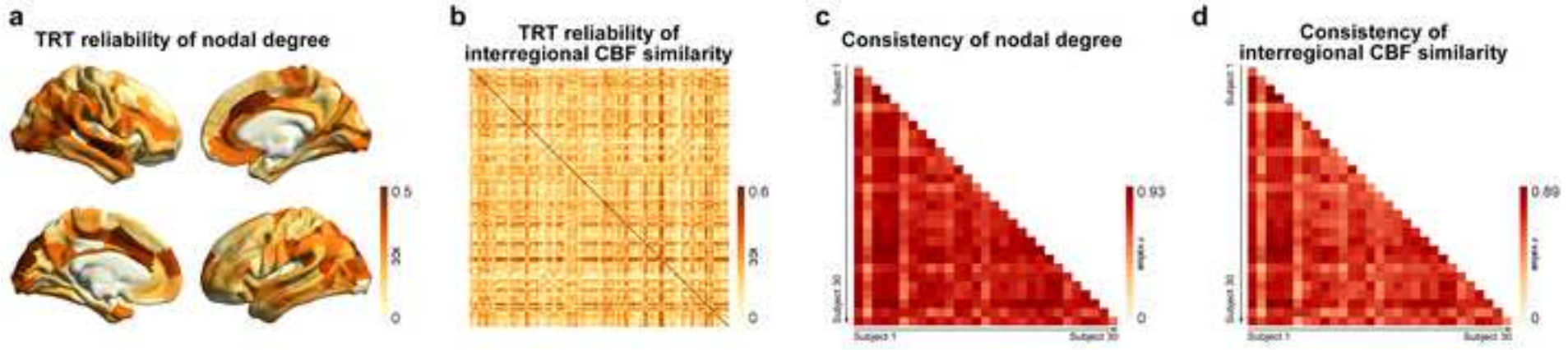

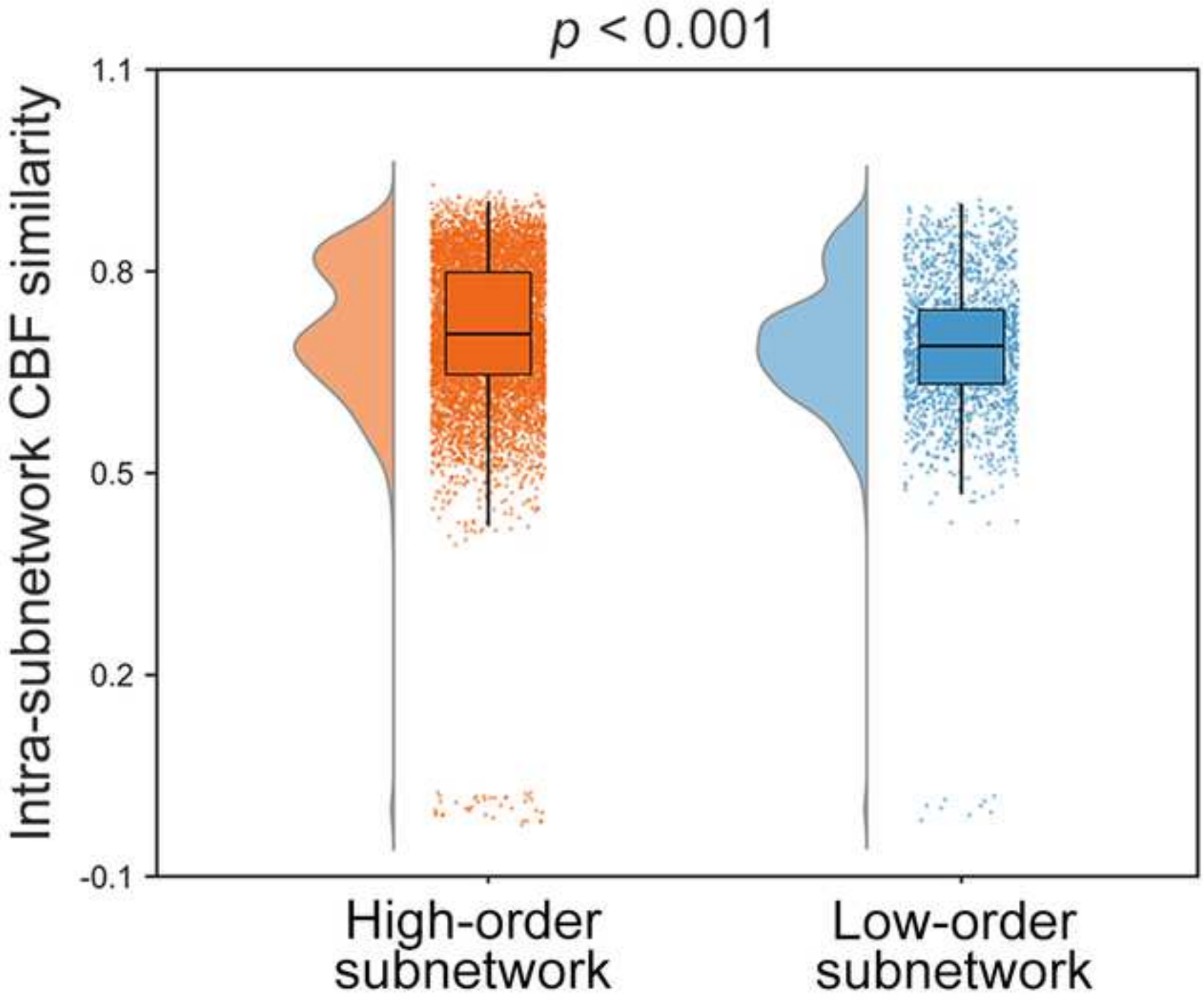

9. Figure

Click here to access/download;9. Figure;Figure4.tif

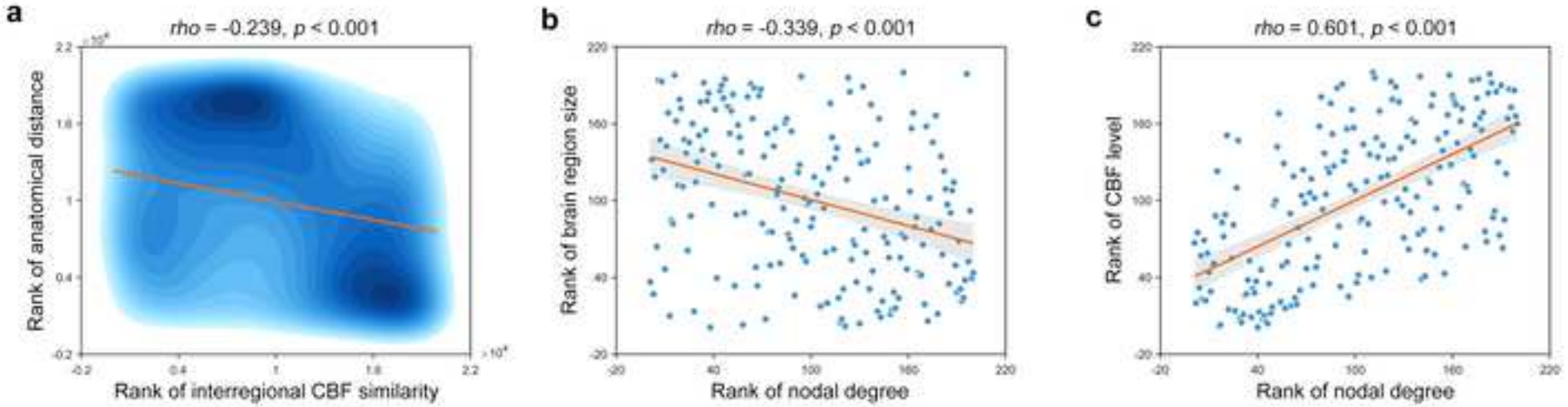

9. Figure

Click here to access/download;9. Figure;Figure5.tif

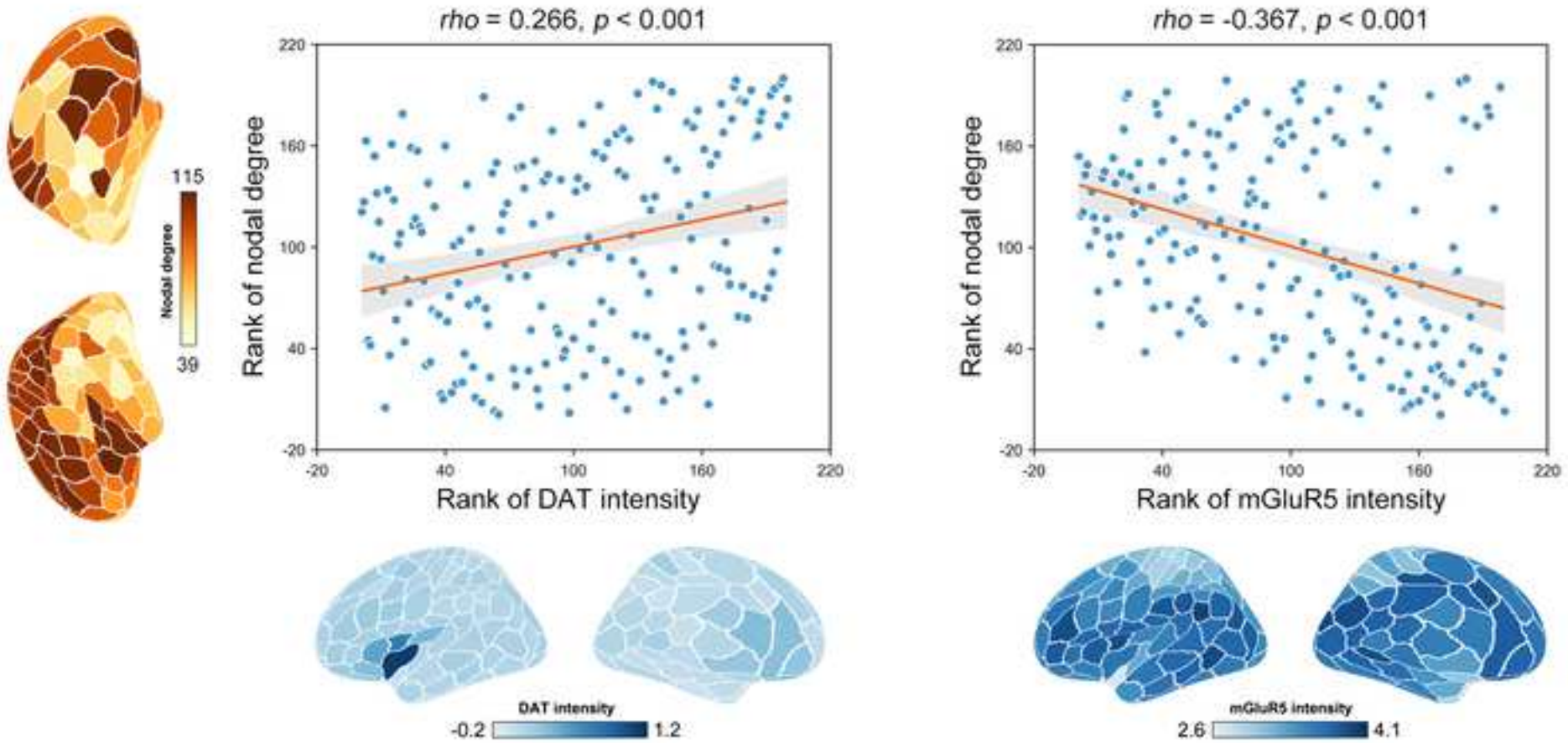

9. Figure

Click here to access/download;9. Figure;Figure6.tif